Proceedings of the Sixteenth (2006) International Offshore and Polar Engineering Conference
San Francisco, California, USA, May 28-June 2, 2006

ISBN 1-880653-66-4 (Set); ISSN 1098-6189 (Set)

Wave Energy Transformation Processes in a Low-energy Mediterranean Surf Zone

Simone Caleffi, Paolo Ciavola

Dipartimento di Scienze della Terra, Università di Ferrara
Ferrara, ItalY

ABSTRACT

The dissipation and distribution of wave energy was investigated on a transect crossing the surf zone. The site is a fine grained, gently sloping beach near the river mouth of Fiumi Uniti, in the Upper Adriatic Sea. A method is described here to determine the frequency cut-off between the infragravity and the sea-swell frequency band, using the cross-shore evolution of the surface Energy Density Spectra (EDS). The temporal variations in infragravity levels were strongly related to those in incident wave energy, even if not affected by dissipation during the propagation. The analysis also considered the correlation between the incident wave height and the cross-shore current. The results cannot often find a confirmation with previous works, because of differences in the environmental setting, with small short-crested waves and limited tidal excursion.

KEY WORDS: wave spectrum; cut-off frequency; energy dissipation; infragravity band; cross-correlation function.

INTRODUCTION

Coastal and sedimentary processes have nowadays become an important subject of study even for local political administrations; the economic value of a healthy beach is of primary importance in coastal zone management.
One of the most relevant factors that control coastal morphologic changes is the impact of storms. Local current circulation and sediment transport are mostly due to breaking waves, the turbulence generated by waves in the surf zone can lift the sand, while longshore currents or rip currents can drag it away. The surf zone is characterized by a complex interaction of wave induced fluid motions such as high frequency turbulence, wave induced currents and infragravity waves. With the Fourier analysis the signal elevation record can be transformed into a frequency domain, creating an easier way to analyze the time signal. Sea-swell waves generally have small to medium wave periods, so that their domain is located in the high frequency band of the spectrum; conversely, infragravity waves have longer periods, from 20 up to hundreds of seconds, therefore they are located in the lowest part of the spectrum. Infragravity wave energy is weakly dissipated in the surf zone, providing a theoretical explanation for many nearshore morphological features including multiple longshore bars, rhythmic forms and other irregularities in the coastline position (Bowen and Inman, 1971; Short, 1975; Bowen, 1980; Holman and Bowen, 1982). In addition, infragravity waves may contribute to shoreline erosion during storms, since a large part of the offshore suspended sediment transport can occur at infragravity frequencies (Beach and Sternberg, 1991). The energy level in the lower part of the spectrum is forced directly or indirectly by the sea-swell band; normally the infragravity wave height is 10-50% of the incident wave height. The importance of the infragravity wave motion increases in the onshore direction. For example, the wave run-up is often dominated by low frequencies, because of the energy conservation trough the surf zone; on the other hand infragravity waves are independent of the local water depth. The separation of high from low frequencies allows the study of different kinds of waves with different energy behavior. At present there is no agreement about the definition of a cut-off frequency to divide the spectrum. The purpose of this paper was to determine the distribution of wave energy, in both the infragravity and the sea-swell frequency bands, processing two distinct elevation signals recorded at the same time on a cross-shore transect.

AREA CHARACTERISTICS AND EQUIPMENT

The study area (Fig. 1) is located north of Lido di Dante (Ravenna), the site is a fine grained, gently sloping beach, positioned between the Fiumi Uniti river mouth and an embankment that protects cultivated fields. The place is influenced both by marine and fluvial processes.
During the field work data was obtained using two distinct time-synchronized measuring platforms. Both instrument sets were equipped with a biaxial current meter, a pressure transducer and a data-logger.

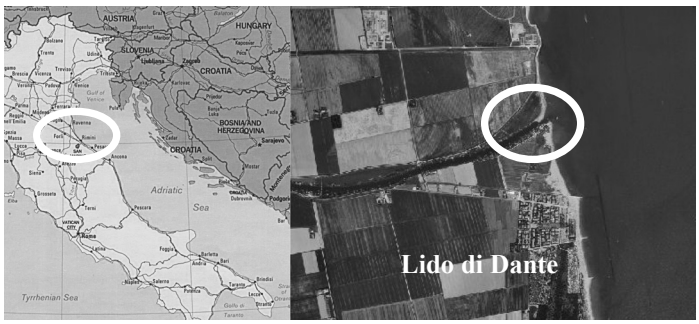

Fig. 1. Study site in the area of Ravenna, north of The Fiumi Uniti. Aerial image from flight AIMA 1996, © CGR Parma.

One data gauge was a SLOT unit (by VALEPORT LTD) working with a sample frequency of 2 Hz capturing one burst every hour, with a length of 20 minutes. The second gauge was an S4 (S4ADWI by Inter Ocean System) programmed as the SLOT unit, to permit data comparison. The two rigs were deployed along a cross-shore transect to avoid any kind of energy loss but the bottom friction during on-shore wave propagation.
The SLOT unit was installed during low tide at a mean water depth of 1.3m, while the S4 was deployed from a boat at a mean water depth of 2.5m (Fig. 2).

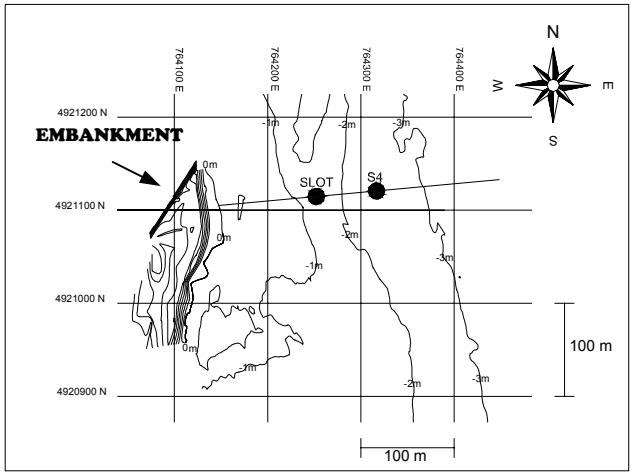

Fig. 2. Nearshore bathymetry of the site and location of the sensors. Coordinates in the UTM system.

INITIAL DATA SETS

Due to the different date of installation of the two gauges (SLOT on 18 April 2004 and S4 on 19 April 2004), only 69 bursts could be compared, captured between 19 April 2004 at 11 a.m. and 22 April 2004 at 7 a.m. Using the SLOT burst numeration system, this period spaces from burst number 19 till number 87.
Figures n.3 and n.4 represent the wave direction versus the peak period and the tide oscillation versus the significant wave height (H_s), both measured at the outer station (S4). It clearly appears that the wave climate did not present constant characteristics in wave height with no trends linked to the tidal variations. Small storm peaks were generated by low intensity local climatic conditions.

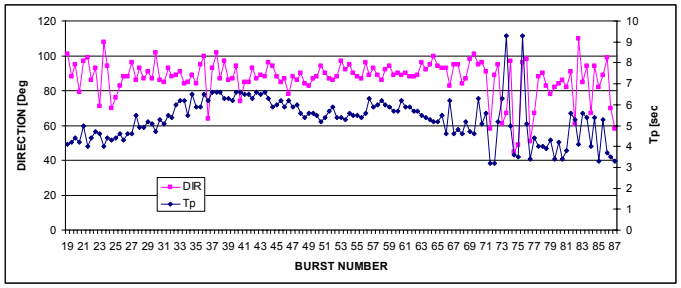

Fig. 3. Burst averaged wave direction and peak period at the outer station.

Two wave height peaks over 70 cm are due to distinct storm phenomena measured at the beginning of the record interval. A progressive decrease in wave energy conditions occurred instead towards the end of the experiment.

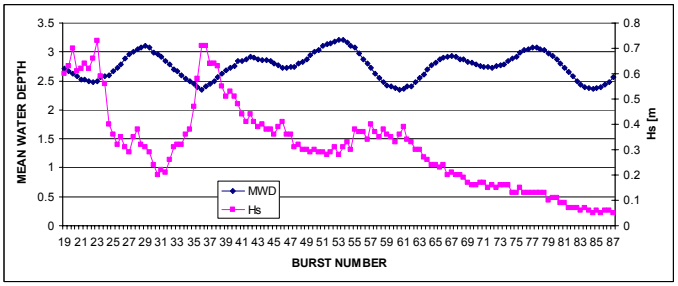

Fig. 4. Burst averaged water depth and significant wave height at the outer station.

After processing the wave signal using the Fast Fourier Transform (FFT), a small amount of energy is seen to be present in the low frequency band of the spectrum, that corresponds to the infragravity wave energy domain. In Fig. 5 is an example of two simultaneous bursts recorded at the outer (S4) and inner station (SLOT). The resemblance between the two spectral shapes is clear, but the peak energy level decreases significantly moving inshore.

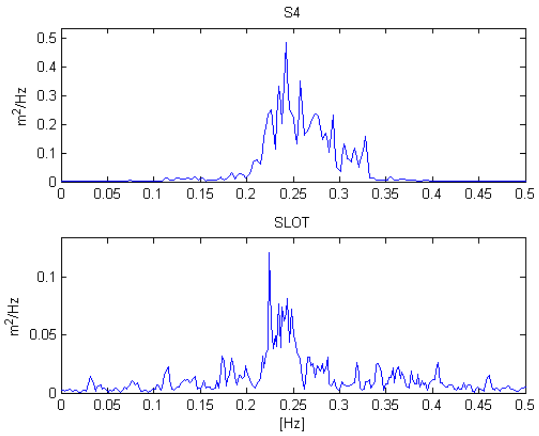

Fig. 5. Wave spectra measured at the outer and inner station (burst n.19)

METHOD OF DATA ANALYSIS

The equation that exponentially connects the total energy level to the significant wave height (H_s) can be expressed as:

$$E = \frac{1}{16}\rho g\, H_S^2 \tag{1}$$

where E is the energy, g the gravitational acceleration and ρ is the water density. The following notations are introduced to analyze separately the two frequency bands, in the two cases of high (hi) and low (lo) frequencies:

$$H_{lo} = 4*\left[E_{lo}\right]^{\frac{1}{2}} = 4*\left[\int_{Flo}^{Fc} s(f)\,df\right]^{\frac{1}{2}} \tag{2}$$

$$H_{hi} = 4*\left[E_{hi}\right]^{\frac{1}{2}} = 4*\left[\int_{Fc}^{Fhi} s(f)\,df\right]^{\frac{1}{2}} \tag{3}$$

where s(f) is the energy density associated to the frequency f, Fc is the frequency cut-off between the infragravity and the sea-swell band.
At the moment there is no agreement in setting the point of cut-off as a fixed value on the frequency axis (Herbers et al., 1995; Raubenheimer et al., 1996; Holland and Holman, 1999), some authors, like Roelvink and Stive (1989) fix this value as a multiple of the peak frequency. Because of a weak sea state and of the absence of a defined energy peak, a fixed value of this frequency could not be accepted. A rational method (Sénéchal et al., 2001) was applied to analyze the sea-swell separately from the infragravity band. The cut-off frequency was determined (Fig. 6) observing the ratio between the EDS_{off} (S4) and the EDS_{int} (SLOT).

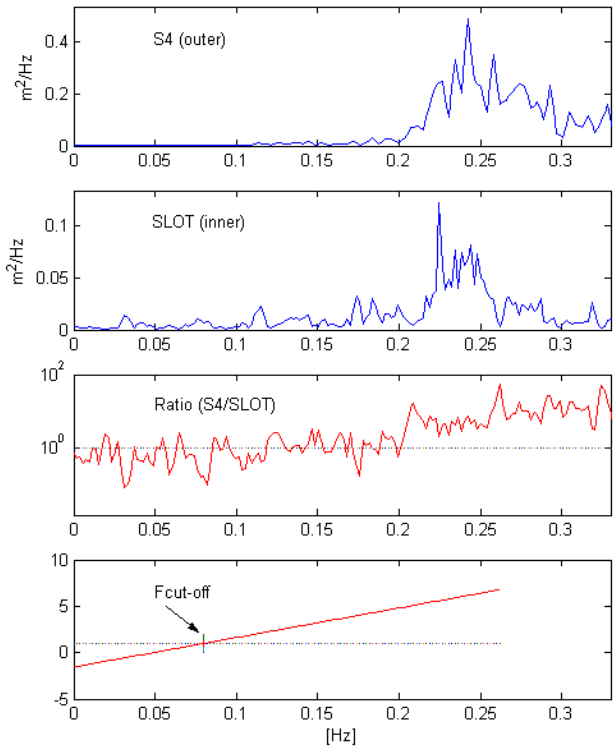

Fig. 6. Wave energy distribution and chosen cut-off frequency (burst n.19).

If one remembers the characteristics of the two frequency bands, sea-swell waves are depth limited, so they dissipate energy traveling landward. Infragravity waves are independent of the water depth (due to their long period and wave length) conserving or increasing energy during the propagation (Wright et al., 1982; Ruessink, 1998).
A value of the ratio EDS_{off} / EDS_{int} below 1 indicates that a higher energy level is present at the inner station than at the outer one, thus the energy increases during the propagation on-shore. On the other hand, when the value of the ratio shifts above 1 it means that a loss of energy occurred during the propagation in the surf zone. In theory, when the ratio has exactly the value 1, there is no energy variation, and the corresponding frequency value should be the cut-off frequency. In practice it is not so easy to find this point on the frequency axis, because of oscillations around the value 1. If the ratio curve is interpolated with a line, its intersection with the horizontal line of value 1 is easier to recognize (Fig. 6). All the computations for the 69 bursts have been averaged to obtain a cut-off frequency with a value of 0.07 Hz.

THE SEA-SWELL BAND

From Fig. 4 it is possible to notice the absence of constant characteristics in wave height because of local meteorological conditions, like weak intensity storms or variable winds. Therefore, the whole data set was divided and grouped into two temporal segments with some analogies. From burst number 38 to 53 (segment A), and from burst number 60 to 79 (segment B), some common features are present, such as the loss of wave height as the tide is growing. Both the segments also show a similar correlation between wave height and water depth (Fig. 7).

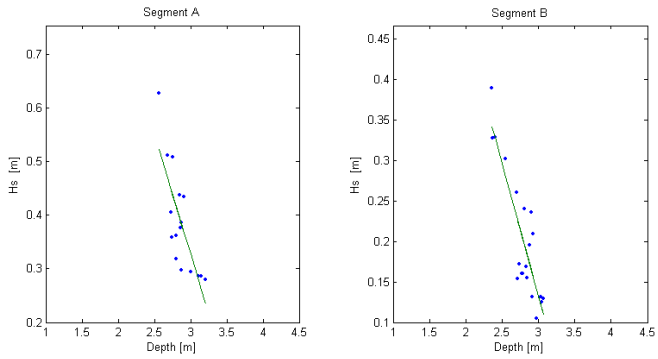

Fig. 7. Least squares linear regression for both the segments between Hs and D.

The ratio between H_s and the water depth, the relative wave height ($\gamma = H_s/D$), never exceeds 0.25; in this case, the outer station (S4) can be considered with good approximation outside the surf zone. The least squares linear fit to the data results to be:

Segment A: $H_s = 1.6 - 0.4*D$ (R=0.79) (4)

Segment B: $H_s = 1.1 - 0.3*D$ (R=0.88) (5)

where D is the water depth.

Fig. 8 represents the γ (H_s/D) value versus the normalized beach slope $\beta/(kD)$, where β (0.02) is the value obtained from a topographic survey undertaken during the experiment and k is the wave number.

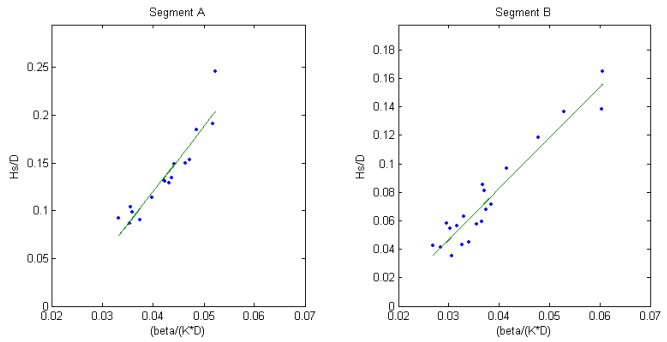

Fig. 8. Least squares linear regression for both the segments between γ and β/(kD).

The least squares linear fit is:

Segment A: $\gamma = 5.8*[\beta/(kD)] - 0.12$ (R=0.95) (6)

Segment B: $\gamma = 4.9*[\beta/(kD)] - 0.09$ (R=0.94) (7)

The high values of the R coefficients demonstrate the good correlation between the variables, but the relationship found does not agree with previous works on dissipative beaches, with higher wave energy conditions and using different cut-off frequency values (Raubenheimer et al., 1996; Sénéchal et al., 2001), so that a universal parameterization based on a linear relation between γ and β/(kD) is probably not valid. In the following figure (Fig. 9) is shown the superimposition of the work of this paper with results of previous authors.

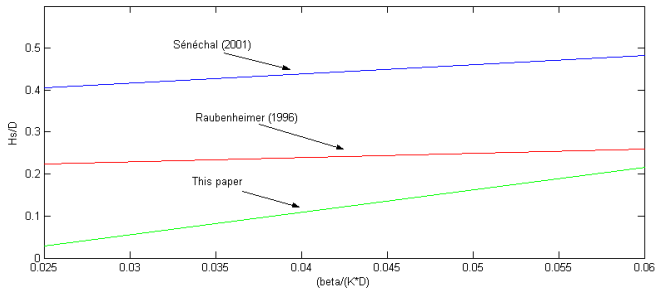

Fig. 9. Superimposition of different results of previous authors.

RELATIONSHIP BETWEEN THE ENERGY BANDS

A large number of field experiments show that the energy level in the infragravity band is strongly correlated with the sea-swell frequency; while the amount of energy in the upper band is dissipated, the infragravity energy grows trough the surf zone (Wright et al., 1982; Ruessink, 1998). The real mechanism of infragravity generation is still unknown, but ascribing its generation to breaking processes is generally considered possible (Ruessink, 1998).

The whole amount of energy contained in the 69 bursts at the outer station (S4) is 5.58 kJ/m^2 (energy per surface unit), of which 98% is contained in the sea-swell frequency band, while just the 2% is stored in the low frequency segment. At the inner station the total energy is 1.05 kJ/m^2, 89% in the upper band, 11% at the lower frequencies (Table 1).

Table 1. Energy divided in spectral bands for the inner (SLOT) and outer (S4) station.

	S4 [kJ/m^2]	SLOT [kJ/m^2]	S4 [%]	SLOT [%]
E. High	5.47	0.93	98 %	89 %
E. Low	0.11	0.12	2 %	11 %
E. TOT	5.58	1.05		

It is evident how there is no energy loss in the infragravity band, contrary to the high band that has dissipated a large amount of energy in the surf zone.

In the following graphs (Fig. 10 and 11), the energy evolution shows the correlation between the two frequency domains of the spectrum, at both stations. The relationship between the two energy levels is evident for both cases (for the outer station more than for inner one); the ratio between high and low energy indicates a scale factor, different for the two positions but constant during the experiment, equal to ~100 for the S4 and to ~10 for the SLOT.

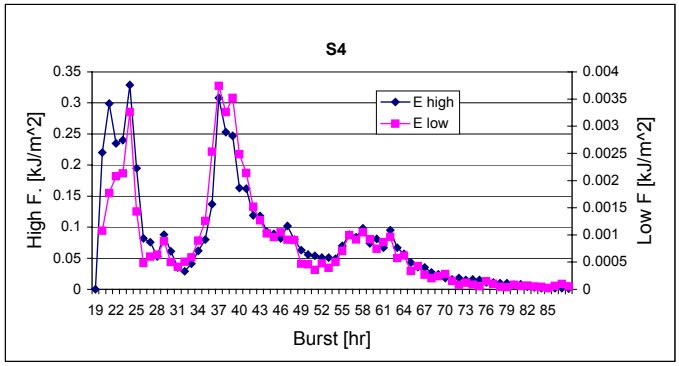

Fig. 10. Distribution of the sea-swell and infragravity energy for the outer station (S4).

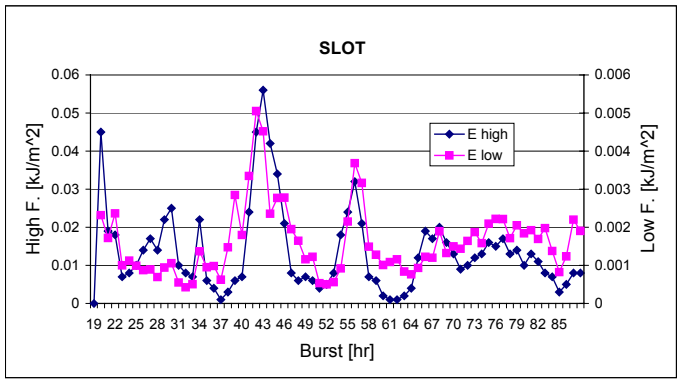

Fig. 11. Distribution of the sea-swell and infragravity energy for the inner station (SLOT).

The time-series evolution (Fig. 12) of the ratio between high frequencies (E-high-S4 / E-high-SLOT), and low frequencies (E-low-S4 / E-low-SLOT) shows that the loss of energy at high frequencies (due to short-crested waves at breaking conditions) is opposite to the behavior of low frequencies.

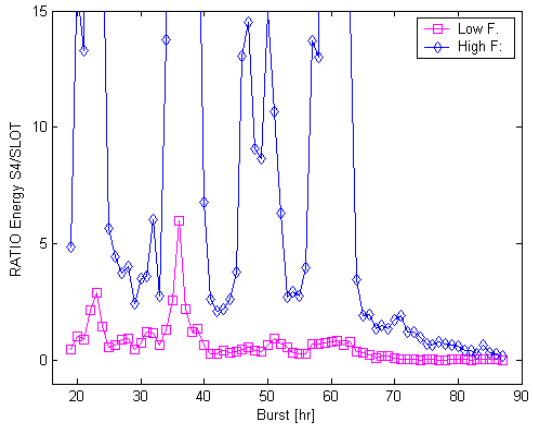

Fig. 12. Trend of the ratio (S4/SLOT) between sea-swell and infragravity energy.

A link between the low and the high frequencies was also investigated, for both the instruments, but with no results. As it is shown in the next figure (Fig. 13), the data dispersion does not permit a significant linear fitting.

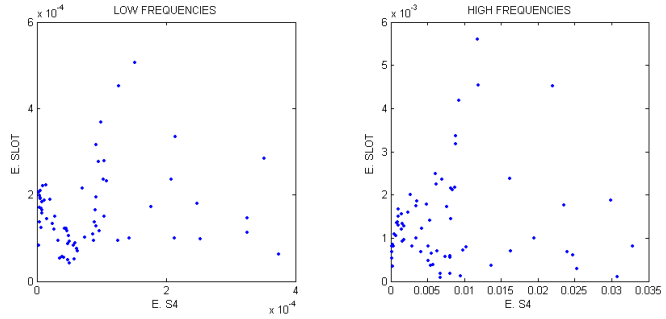

Fig. 13. Absence of a link between the low and the high frequencies.

A significant relationship was found between the energy levels in the two different bands. The results (Fig. 14) for the S4 station are more significant than for the SLOT (the correlation coefficient is higher), because of its position out of the surf zone (not disturbed by wave breaking).

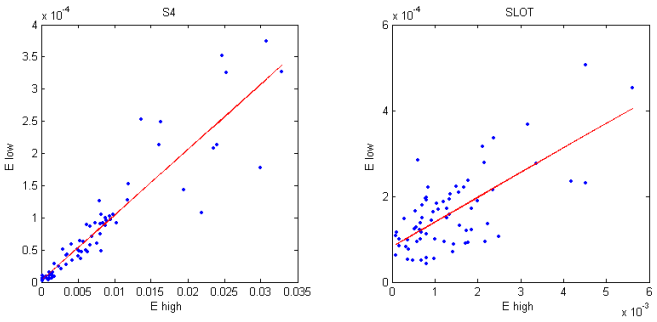

Fig. 14. Least squares linear fit to the data at the outer and the inner station (respectively S4 and SLOT).

The least squares linear fit to the data, pertinent to the S4 outer station, helds:

$$E_{low} = 0.01*E_{high} \qquad (R=0.93) \qquad (8)$$

The least squares linear fit to the data, pertinent to the SLOT inner station, results:

$$E_{low} = 0.062*E_{high} + 0.0001 \qquad (R=0.72) \qquad (9)$$

Contrary to the relation carried out for the outer station, in the case of energy absence on the high frequencies, a small amount of energy remains in the infragravity band. This could be an evidence of entrapped energy due to edge waves that travel in the surf zone.

Repeating the analysis on the bursts for segments A and B, the results become even more significant, because of the similar wave and tide conditions.

A higher sea-swell wave height characterizes segment A; an averaged ratio nearly equal to 7 is computed from the outer to the inner station. This value indicates a loss equivalent to 85% of the initial energy recorded at the S4 station. Contrary to this trend, as expected, the infragravity band shows an increase approximately equivalent to 100% from the S4 to the SLOT station.

Segment B is characterized by a smaller significant wave height. The behavior of this second segment confirms the trend reported for the first one, but such a small wave height, decreasing to few centimeters, lets even the inner station out of the surf zone, so that a comparison between the infragravity band and the sea-swell frequency does not seem significant.

The correlation between the two distinct energy bands in segments A and B is shown below (Fig. 15 and 16).

The least squares linear fit to the data, regarding the S4 station, results:

Segment A: $E_{low} = 0.016*E_{high}$ (R=0.99) (10)

Segment B: $E_{low} = 0.01 *E_{high}$ (R=0.96) (11)

For the SLOT station, the correlation is significant just for segment A (for segment B the correlation coefficient is less than 0.5). The least squares linear fit to the data, regarding the SLOT station, results:

Segment A: $E_{low} = 0.066*E_{high} + 0.0001$ (R=0.80) (12)

Considering the whole data set and the A and B subsets, some resemblances and some differences are noted. A strong relationship is clearly present between the two energy bands recorded at the outer station, the correlation coefficient value is always greater than 0.9. On the other hand, this value is not often so significant at the SLOT position, mainly because of the low energy conditions of the terminal part of segment B.

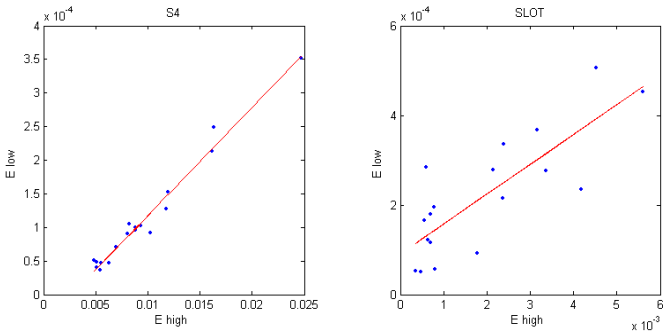

Fig. 15. Segment A, correlation between the two distinct energy levels.

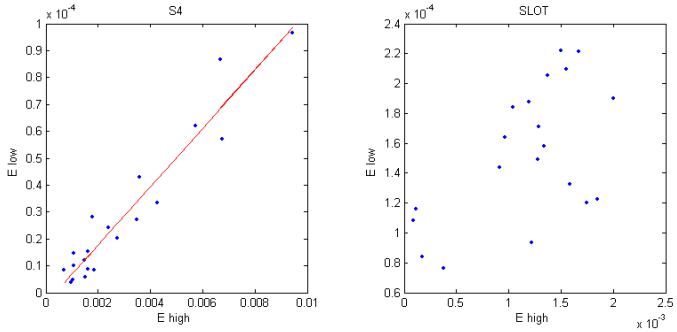

Fig. 16. Segment B, correlation between the two distinct energy levels.

WAVE-INDUCED CURRENTS

Surf zone currents are generated by wave action in and near the breaker zone and are almost exclusively due to energy dissipation by breaking waves (Aagaard and Masselink, 1999; Aagaard and Bryan, 2003). To simplify the analysis, surf zone currents were decomposed along two directions, perpendicular and parallel to the shore.

The current signal was available just at the inner station SLOT, and the data were processed by spectral analysis. From the analysis of the averaged long and cross-shore current versus the mean water depth (Fig. 17), a repetitive trend is present till burst n. 66 (when H_s decreases below 20 cm). At low tide the cross-shore current is directed seawards (negative values), while the longshore current velocity presents a northward direction (positive values). The averaged longshore current never exceeds 35 cm/sec, while the cross-shore current is always smaller than 15 cm/sec.

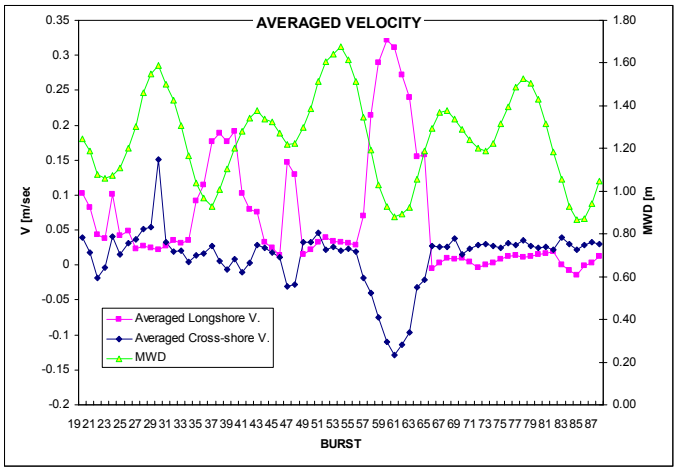

Fig. 17. Averaged long and cross-shore current velocity correlation with tide oscillation.

A larger standard deviation of the cross-shore readings with respect to the longshore current (Fig. 18) confirms that the incoming wave direction was almost normal to the beach. Therefore it seems likely that the longshore currents were tidally generated.

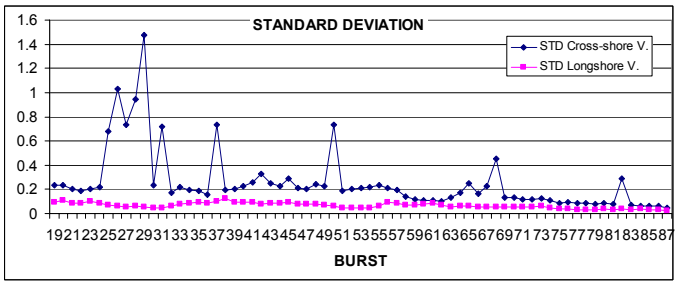

Fig. 18. Long and cross-shore current standard deviation

The first group of observations regard the difference between the peak spectral energy levels in the cross-shore and longshore spectra; the cross-shore energy is often one order of magnitude bigger than the longshore component (Fig. 19).

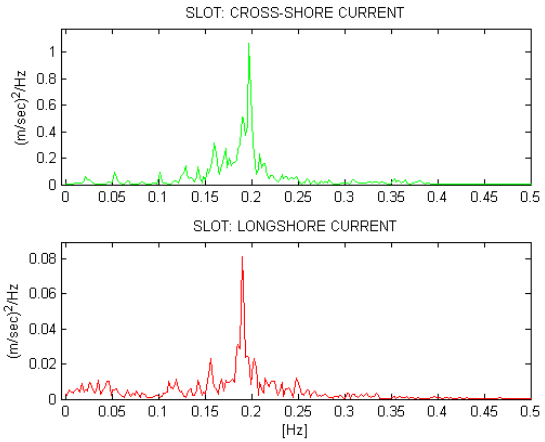

Fig. 19. Example of cross-shore and longshore current spectra at the SLOT inner station (burst n.31).

In fact, the incident wave direction varied within narrow limits around the direction normal to the beach, determining the predominance of a cross-shore component.

In the bursts with higher energy, the peak energy is confined in the range 0.5-1.5 $(m/s)^2/Hz$, with predominant energy between 0.20 and 0.25 Hz; the longshore current shows best agreement with the cross-shore component, around high tide.

The cross-correlation function (Fig. 20) was used to quantify the existing relation between the wave elevation signal and the cross-shore current signal. It seems to be a robust tool to understand and quantify the lag and the likeness between the two signals. The highest positive peak in the oscillating function is a quantifier of the signal similarity; the secondary positive peaks of the function, usually one backward and one forward, symbolize the possibility of a second signal superposition at different time steps. The secondary positive peaks are smaller than the main peak, stating that the two signals can be superimposed shifting the initial starting time of one signal backward or forward. The larger is the value of the peak, included in the range [0-1], the larger is the resemblance between the signals. The lag value corresponding to the highest peak of the cross-correlation function, showing the delay of the current induced by the waves; a lag unity corresponds to a sample frequency at the chosen interval (2 Hz).

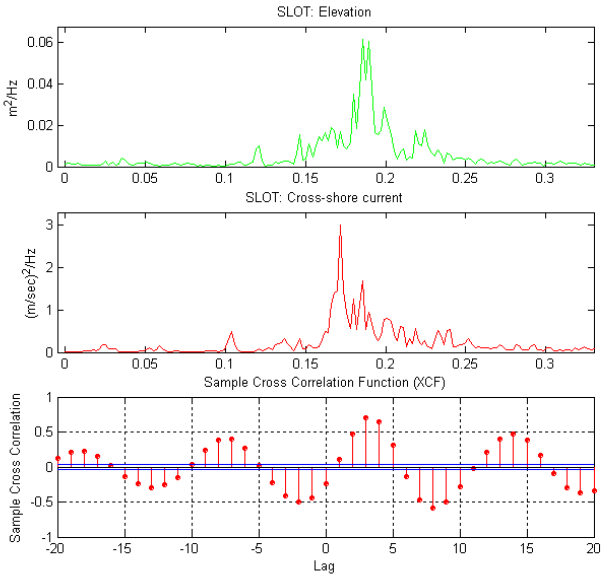

Fig. 20. Example of EDS and cross correlation function between the elevation and cross-shore current record (burst n. 53).

In the case of a rising tide, the presence of energy is noted on a narrower range on the frequency axis. With a higher water column on the instrument, the increasing value of the ratio h/L results in a lower interaction between the waves and sea bottom. Spectra usually have the energy peak in the range between 0.1 e 0.3 Hz. At high tide, with a well-defined energy density peak, an increased value of the secondary peaks in the cross-correlation function is noted. Considering all the obtained cross-correlation functions, the trend of the main peak value is represented in the figure below (Fig. 21). Excluding the final part of the experiment (low energy conditions), a large number of bursts have the max peak higher than 0.5, confirming the good correlation level.
The lag between waves and induces currents is constant in the whole data set, shifting its value between 3 and 4 lag units.

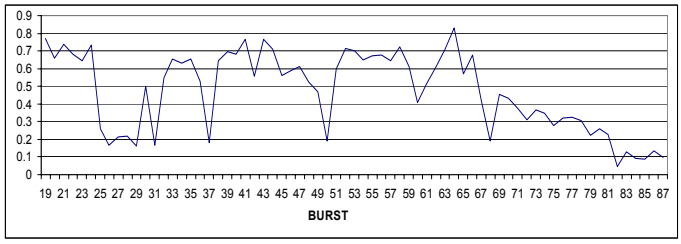

Fig. 21. Maximum cross-correlation peak values.

The oscillations of the secondary peaks were then analyzed in terms of amplitude and period. The graph in figure 22 shows the almost-symmetrical trend of the period, understood as the lag-distance, between the two secondary peaks of the cross correlation function. The enlargement (or the restriction) of the hatched area can be read as an increase (or a decrease) of the time interval that makes the signals overlapping.

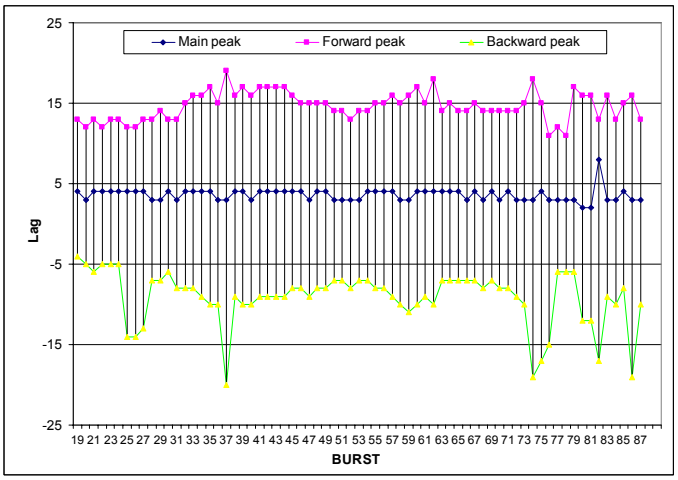

Fig. 22. Trend of the period (lag-distance) between the two secondary peaks of the cross correlation function.

Another consideration can be made on the cross-correlation function about the secondary peak value. Figure 23 presents a good superposition between the two positive secondary peaks (backward and forward). Moreover, in the higher energy conditions, the trend of these values follows the oscillation of the tide.

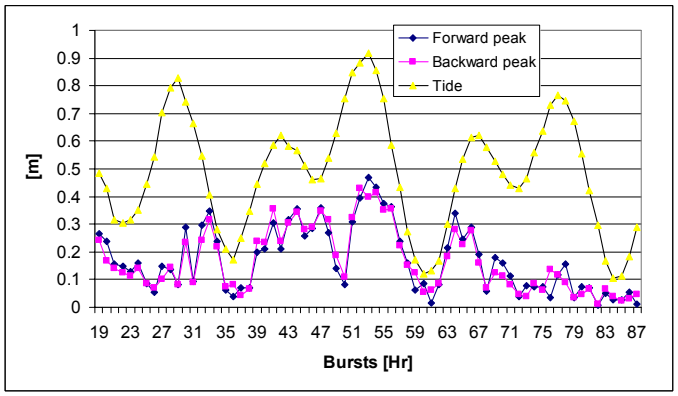

Fig. 23. Superposition of the secondary cross-correlation peaks versus the tide oscillation.

In summary, during the transition from low to high tide, the energy density spectra tighten their width, forming a well defined energy peak, while the cross-correlation functions increase the amplitudes of the secondary peaks.

CONCLUSIONS

Data recorded from the two rigs, S4 e SLOT, made possible the analysis of the energy spectra evolution along a cross-shore transect. Each spectrum was divided into two different bands, separating the sea-swell frequency from the infragravity one, setting the cut-off frequency at 0.07 Hz. The applied method, based on the variation of the spectral density energy ratio EDS_{off}/EDS_{int}, seems to be a good criterium to separate the spectrum in two different frequency bands. The results obtained from the analysis of the sea-swell band show a depth-limited behavior and a good correlation between γ and $\beta/(kD)$, even if the linear regression through the data differs from previous works on high energy dissipative beaches. Analyzing separately the low from the high frequencies, the independence of infragravity motions from the local water depth is demonstrated during shoreward propagation, because of

energy conservation, contrary to the sea-swell band that dissipates a large amount of energy. Moreover, the link between the two energy bands was found and quantified, showing that the ratio between the energy levels remained constant in time but not in space. The scale factor that linked the different energy bands was correlated to the sensor's position (thus depending from local water depth).

The relationship between wave elevation and cross-shore current at the inner station (SLOT) was investigated with a cross-correlation function. A constant lag was found between the signals and during the passage from low to high tide. Around high tide the energy density spectra tightened their energy band shaping a better defined energy peak. Wave reflection on the shore could an hypothesis to explain the phenomena: under low to medium water depths along the tidal cycle the flooded part of the beach had a low gradient, therefore a dissipative behavior, with dominant energy dissipation. Once the water depth approaches high tide the upper part of the beach is flooded: this has a steeper slope, causing a more reflective conditions.

Future work will try to evaluate the role of these processes in sediment suspension, its lateral advection and the associated morphological changes.

REFERENCES

Aagaard, T, and Bryan, KR (2003). "Observation of infragravity wave frequency selection," *Continental Shelf Research*, Vol 23, pp 1019-1034.

Aagaard, T, and Masselink, G (1999). "The Surf Zone," in Short AD (ed.), *Handbook of Shoreface Morphodynamics*. Wiley & Sons, Chicester, UK, pp. 72-118.

Beach, RA, and Sternberg, RW (1991). "Infragravity driven suspended sediment transport in the swash, inner and outer-surf zone," *Proceedings Coastal Sediments 1991*. American Society of Civil Engineers, New York, USA pp 114-128.

Bowen, AJ (1980). "Simple model of nearshore sedimentation: beach profiles and longshore bars," *Geological Survey of Canada,* Paper 80-10, pp 1-11.

Bowen, AJ, and Inman, DL (1971). "Edge waves and crescentic bars," *Journal of Geophysical Research,* Vol 76, pp 8662-8671.

Hegge, BJ, and Masselink, G (1995). "Spectral analysis of geomorphic time series: auto-spectrum," *Earth Surface Processes and Landforms*, Vol 21, pp 1021-1040.

Herbers, THC, Elgar, S, Guza, RT, O'Reilly, WC (1995). "Infragravity frequency (0.005-0.05 Hz) motions on the shelf," *Journal of Physical Oceanography*, Vol 25, pp 1063-1079.

Holland, KT, and Holman, RA (1999). "Wavenumber-frequency structure of infragravity swash motions," *Journal of Geophysical Research*, Vol 104, pp 13479-13488.

Holman, RA, and Bowen, AJ (1982). "Bars, bumps and holes: models for the generation of complex beach topography," *Journal of Geophysical Research,* Vol 87, pp 457-468.

Masselink, G (1994). "Group bound long waves as a source of infragravity energy in the surf zone," *Continental Shelf Research*, Vol 15, pp 1525-1547.

Raubenheimer, B, Guza, RT, Elgar, S (1996). "Wave transformation across the surf zone," *Journal of Geophysical Research*, Vol 101, pp 25589-25597.

Roelvink, JA, and Stive, MJF (1989). "Bar-generating cross-shore flow mechanisms on a beach," *Journal of Geophysical Research*, Vol 94, pp 4785-4800.

Ruessink, BG (1998). "The temporal and spatial variability of infragravity energy in a barred nearshore zone," *Continental Shelf Research*, Vol 18, pp 585-605.

Sénéchal, N, Dupuis, H, Bonneton, P, Howa, H, Pedreros, R (2001). "Observation of irregular wave transformation in the surf zone over a gently sloping sandy beach on the French Atlantic coastline," *Oceanologica Acta*, Vol 24, n°6, pp 545-556.

Short, AJ (1975). "Multiple offshore bars and standing waves," *Journal of Geophysical Research*, Vol 80, pp 3838-3840.

Wright, LD, Guza, RT, Short, AD (1982). "Dynamics of a high-energy dissipative surf zone," *Marine Geology*, Vol 45, pp 41-62.